Nanostructured Surface Functionalization of Polyacrylamide Hydrogels Below the Length Scale of Hydrogel Heterogeneity

Juan C. Arango†, Laura O. Williams†, Anni Shi†, Anamika Singh†, Emmanuel K. Nava†, Racheal V. Fisher†, Joseph A. Garfield†, Shelley A. Claridge*,†,§

†Department of Chemistry, Purdue University, West Lafayette, Indiana 47907
‡Weldon School of Biomedical Engineering, Purdue University, West Lafayette, Indiana 47907
Address correspondence to: claridge@purdue.edu, (phone) 765-494-6070

ABSTRACT: Hydrogels are broadly used in applications where polymer materials must interface with biology. The hydrogel network is amorphous, with substantial heterogeneity on length scales up to hundreds of nanometers, in some cases raising challenges for applications that would benefit from highly structured interactions with biomolecules. Here, we show that it is possible to generate ordered patterns of functional groups on polyacrylamide hydrogel surfaces. We demonstrate that when linear patterns of amines are transferred to polyacrylamide, they pattern interactions with DNA at the interface, a capability of potential importance for preconcentration in chromatographic applications, as well as for the development of nanostructured hybrid materials and supports for cell culture.

KEYWORDS: polyacrylamide, monolayers, two-dimensional materials, polydiacetylene, surface chemistry, chemical patterning

INTRODUCTION

Controlling the chemistry of hydrogels is important in many applications, ranging from chromatographic separations to the design of cell culture supports and implants for regenerative medicine.[1-3] In some cases, chemistry is altered throughout the hydrogel through the use of new monomers. However, local changes to hydrogel chemistry are also increasingly important. These can include generation of gradient gels to improve chromatographic separation,[4-5] or microscale chemical environments in which local chemistry and mechanical properties impact interactions with cells.[6]

Polyacrylamide (PAAm) is a hydrogel[7-9] that is widely used in protein and DNA chromatography,[4,10] cell culture,[11] and other applications. Gel formation is typically achieved through free-radical polymerization of an acrylamide (AAm) monomer with a bis-acrylamide (Bis) crosslinker.[12] Pore sizes, and thus mechanical properties, can be controlled by adjusting the ratio of acrylate to water (%T), and the ratio of crosslinker to monomer (%C),[13] as shown in Figure 1. Polyacrylamide networks exhibit significant hierarchical complexity at mesoscopic scales (*ca.* 200-500 nm); thus, exerting high-precision control over the surface chemistry of polyacrylamide and similar hydrogels is challenging.

Recently, we have shown that it is possible to generate high-resolution surface patterns on polydimethylsiloxane (PDMS), a hydrophobic polymer with a different crosslinking chemistry and network structure. In this approach, a precision striped polydiacetylene (sPDA) monolayer,[14] composed of functional amphiphiles with a reactive diacetylene (DA) in the alkyl chain, are first assembled on highly oriented pyrolytic graphite (HOPG), as shown in Figure 1a (top). Due to relatively strong alkyl–π interactions, amphiphiles spontaneously assemble in a lying-down orientation, with the alkyl chains parallel to the substrate, generating striped 1-nm-resolution functional patterns with a sub-10-nm pitch.[15-17] These ordered molecular patterns can be photopolymerized by UV irradiation, generating striped arrays of PDAs (Figure 1a, bottom) with the polymer backbones exposed at the interface for further reactions. By controlling monomer structure[15-16,18-21] and assembly conditions,[16,22-24] it is possible to generate nm-resolution functional patterns on HOPG that extend over large microscopic areas,[24-25] and include diverse pattern symmetries[26] and headgroup chemistries[20] that impact macroscopic and nanoscopic wetting,[15,27] and assembly of nano- and microscopic objects at the interface.[14,28-31] Geometrically localized patterns can also be generated by local application of molecules to the surface using microcontact printing.[20]

Functional patterns prepared in this way can be transferred to PDMS during the PDMS curing process, which involves a crosslinking reaction between a vinyl-terminated base polymer and a crosslinker containing reactive Si-H bonds. Curing PDMS in contact with the striped PDA monolayer, then exfoliating, results in transfer of the patterned PDA monolayer to the PDMS surface.[14,19] We have demonstrated that surface functionalization of PDMS enables control over interactions with nanoscale objects (*e.g.* inorganic nanowires)[14] and molecules (*e.g.* polyelectrolytes)[30] in the environment.

Here, we show that it is possible to use a similar process to control the surface chemistry of PAAm (Figure 1b), a hydrophilic gel with a substantially different polymerization process involving *in-situ* radical reaction of a small-molecule monomer to generate the polymer network. When covalently linked linear patterns of amines are transferred to the surface, they can be used to control adsorption of DNA at the interface, laying groundwork for increasingly complex structural assembly at the interfaces.

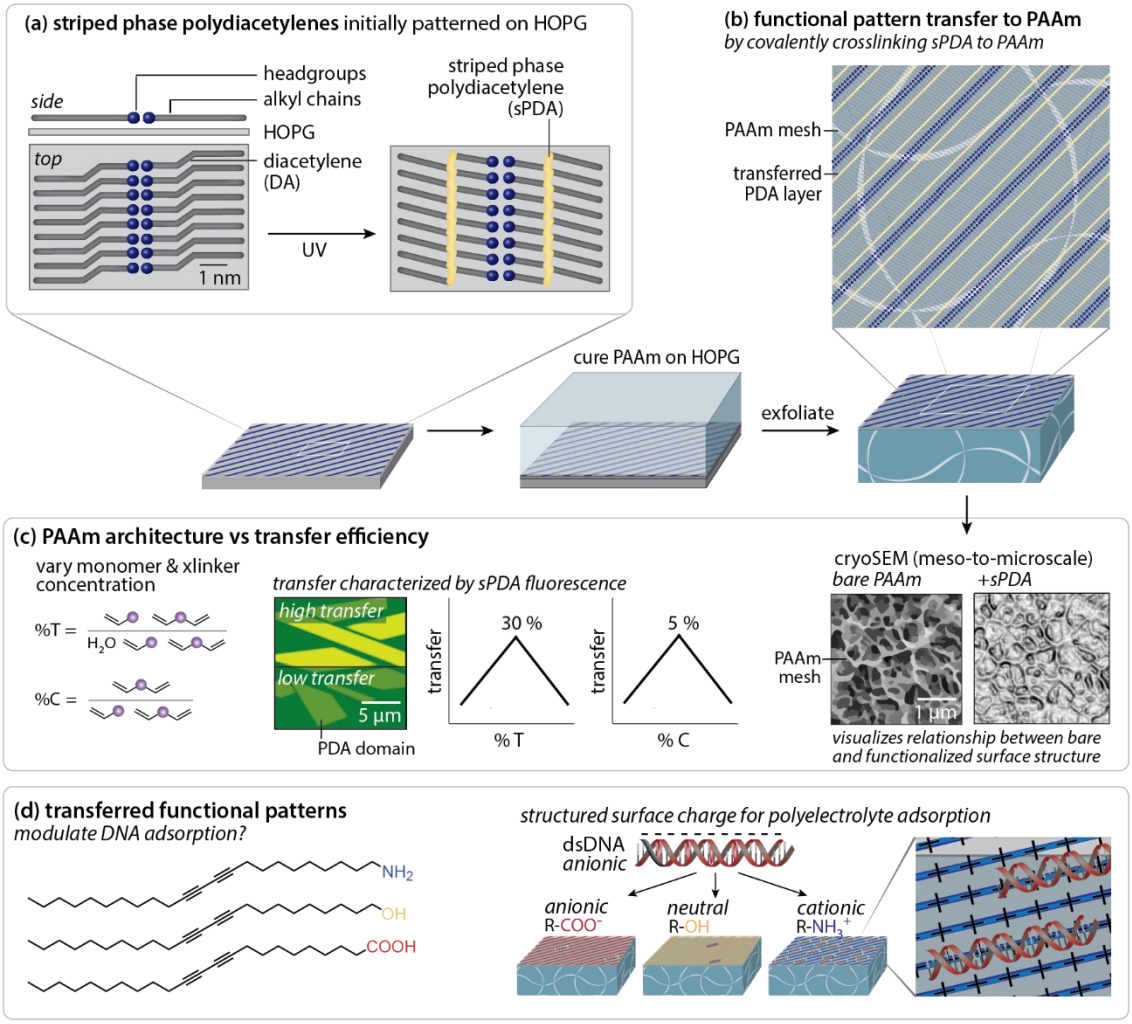

Figure 1. (a) Illustration of sPDA structure on HOPG. (b) Schematic of sPDA transfer to PAAm. (c) Illustration of PAAm compositional variables (%T and %C) that impact transfer efficiency. (d) Illustration of the use of amine sPDAs on PAAm to control DNA adsorption.

RESULTS AND DISCUSSION

Preparation and assembly of striped PDA monolayers on HOPG. Striped PDA (sPDA) monolayers of polymerizable amphiphiles on HOPG (Figure 1,2) were prepared via Langmuir-Schaefer (LS) conversion (see Experimental Methods for details), using methods we have reported previously.[16,21-22] Briefly, LS conversion begins with assembly of a standing phase Langmuir film of amphiphiles on an aqueous subphase. A freshly cleaved HOPG substrate is then slowly lowered into contact with the standing phase monolayer and a subset of molecules in the LS film undergo transfer to the HOPG surface. Under appropriate conditions, the molecules reorient so that the alkyl chains assemble parallel to the HOPG hexagonal lattice (Figure 1a, top), optimizing the relatively strong alkyl–π interactions between molecule and substrate. Monolayers of molecules containing a reactive diyne can then be photopolymerized via UV irradiation to set the molecular pattern (Figure 1a, bottom).

In initial experiments, we utilized sPDAs assembled from 10,12-tricosadiynamine (TCD-NH_2, Figure 2a). Molecules assemble head-to-head, generating lines of functional headgroups ~ 1 nm in width. Energy minimized models (Figure 2b, c) illustrate an edge-to-edge lamellar width of 5.3 nm (Figure 2c) for the polymerized system, in good agreement with the 5.6 nm periodicity observed by atomic force microscopy (AFM), in Figure 2d. During polymerization, the relatively weak amine headgroup dimers can break as the DA rehybridizes to form the PDA, leading to modest variability in the lamellar structure in comparison with COOH sPDAs;[32] here, we illustrate the H-bonded form of the sPDA for simplicity.

While sPDAs are typically studied at nanoscopic scales (<1 µm) by AFM, we have shown previously that scanning electron microscopy (SEM) enables the characterization of molecular ordering over microscopic scales (3–500 µm), commensurate with the scale of fluorescence microscopy images used for characterization on hydrogel surfaces (*vide infra*). In SEM images, stripe phase monolayers locally increase secondary electron generation, creating brighter features in the SEM image that contrast with darker bare HOPG. Molecular orientation in the monolayer is revealed by cracking defects along the lamellar axis (visible in Figure 2e,f), that accumulate due to conformational changes during striped phase polymerization (compare lamellar width in Figure 2b and 2c). See Supporting Information Figure S1 for larger AFM and SEM images.

Transfer of striped phases to polyacrylamide hydrogels. We examined the possibility of transferring sPDAs from HOPG to polyacrylamide (PAAm) hydrogels using *in situ* curing of the bulk polymer, analogous to the process we have demonstrated previously for transfer to PDMS.[14] Polyacrylamide is generated

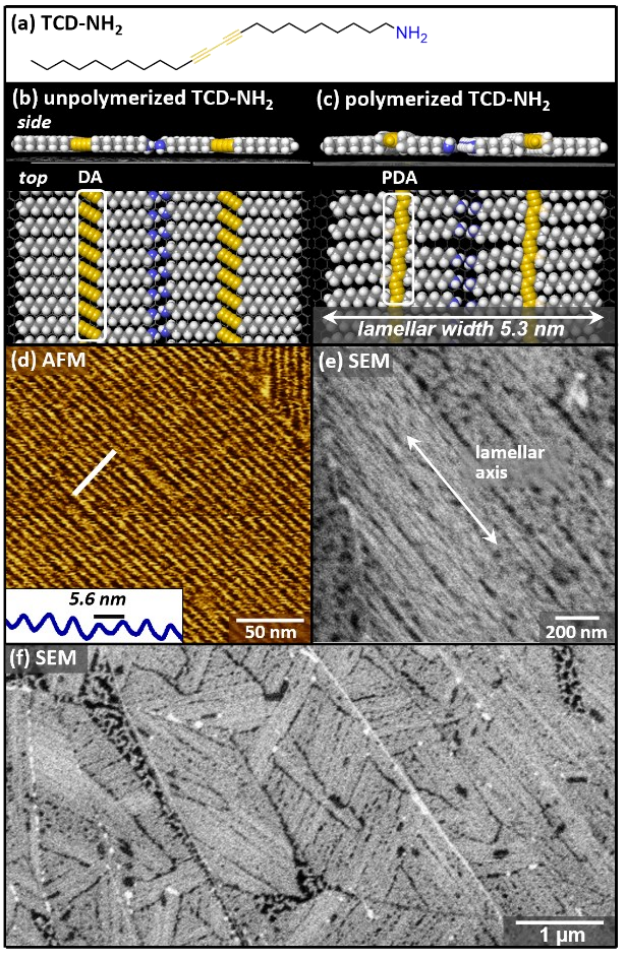

Figure 2. (a) TCD-NH_2 molecular structure; (b, c) Molecular models of (b) unpolymerized and (c) polymerized TCD-NH_2 monolayers on HOPG (TCD-NH_2/HOPG); (d) AFM image of polymerized TCD-NH_2/HOPG showing lamellar periodicity; (e,f) SEM images of microscale TCD-NH_2/HOPG structure.

through a free-radical polymerization of an acrylamide (AAm) monomer, bisacrylamide (Bis) crosslinker, ammonium persulfate (APS) radical initiator and N,N,N',N'-tetramethylethylenediamine (TEMED) radical stabilizer. Here, polyacrylamide reaction mixtures with controlled compositions were cured in contact with sPDA monolayers on HOPG (see Experimental Methods for details).

After crosslinking, the PAAm gel was gently exfoliated from the HOPG substrate (Figure 3a), simultaneously exfoliating any sPDA elements covalently linked to the PAAm. Because the uncured PAAm mixture has low viscosity relative to PDMS mixtures used previously, transfer was carried out by placing a mold with a circular cutout atop the sPDA/HOPG, adding the PAAm mixture, and placing a functionalized glass slide on top of the stack (Figure 3b). Following curing, the PAAm is also covalently linked to the glass slide, which is used as a support (see Experimental Methods for additional details regarding functionalized glass slide preparation, and PAAm curing and transfer).

Previously, we have shown that sPDA fluorescence emission can be used to quantify the extent of sPDA transfer to PDMS.[14,19] Here, we also observe fluorescence emission consistent with sPDA transfer to PAAm. Figure 3c–e illustrates this process using both full sPDA monolayers and square patterns of TCD-NH_2 sPDAs assembled on HOPG by microcontact printing (μCP, see Experimental Methods for details, and larger fluorescence micrographs of both LS and μCP surface preparation, Figure S2) and then transferred. Fluorescence emission spectra acquired over areas with transferred sPDAs (Figure 3e) can be fitted to a primary peak near 548 nm, and a set of longer-wavelength peaks, similar to those we have observed previously for sPDAs transferred to PDMS.[32] In contrast with PDMS, which exhibits background fluorescence at 514 nm, PAAm exhibits a peak near 584 nm (Figure 3e, right panel, grey trace). μCP-TCD-NH_2 fluorescence intensities are lower than those for full TCD-NH_2 sPDA layers (Figure 3e,f), consistent with the smaller average molecular domain sizes achieved by μCP in comparison with LS transfer, and our previous observation that transfer efficiency increases with increasing sPDA length.[32]

Impact of polyacrylamide gel structure on sPDA transfer. We carried out a series of experiments to examine transfer efficiency in relation to PAAm composition. Recently, we have examined the relationship between sPDA polymer length and the efficiency of transfer to PDMS, parameterizing the per-unit reaction probability with the PDA, and the number of linkages to the PDA required to exfoliate it with the bulk PDMS.[32] The previous models were developed by comparing transfer efficiency for molecules with known populations of polymer lengths. Overall, these measurements suggest a 1–2% probability of reaction per PDA unit ($p_{rxn,PDMS}$), and minimum of 2–3 covalent linkages typically required for exfoliation of each sPDA.

PAAm polymerization is different than PDMS crosslinking, in that each AAm or Bis monomer is capable of reacting with the PDA. PAAm gel structure is typically controlled by varying the percentage of reactive acrylate (%T) in the reaction mixture, and the percentage of the acrylate that is crosslinker (%C):

$$\%T = \frac{AAm\ (g) + Bis\ (g)}{Total\ vol\ (mL)} \times 100$$

$$\%C = \frac{Bis\ (g)}{AAm\ (g) + Bis\ (g)} \times 100$$

In these experiments, we used acrylate percentages (%T) from 10–50% and crosslinker percentages (%C) from 1–10%, spanning the range of compositions common for DNA and protein electrophoresis.[33]

Overall, we observed that as %T increases from 10% to 30%, fluorescence emission at $\lambda_{max,PDA}$ increases by a factor of 3, then decreases somewhat as %T increases further (40 and 50%). Similarly, emission at $\lambda_{max,PDA}$ reaches a maximum at %C = 5%, decreasing by a factor of approximately 2 at %C = 1% and 10%. The observed maximum at 5% crosslinker is in line with previous electron microscopy observations of pore structure, which have indicated a minimum in pore size in approximately that range, for acrylate percentages near those used here.[34]

Analysis of cryoelectron microscopy (cryoEM) images (see Supporting Information for details) estimates surface pore diameters ~50 nm for 30 and 40%T gels, which produce higher degrees of transfer in comparison with 10%T gels (Figure 4c). CryoEM images of unfunctionalized PAAm (Figure 4d–f) and TCD-NH_2/PAAm (Figure 4g–i) illustrate smoothing of the gel surface associated with the transfer of the TCD-NH_2 sPDA monolayer, particularly for PAAm compositions that result in high degrees of sPDA transfer based on fluorescence emission. We note that these differences likely reflect changes in the

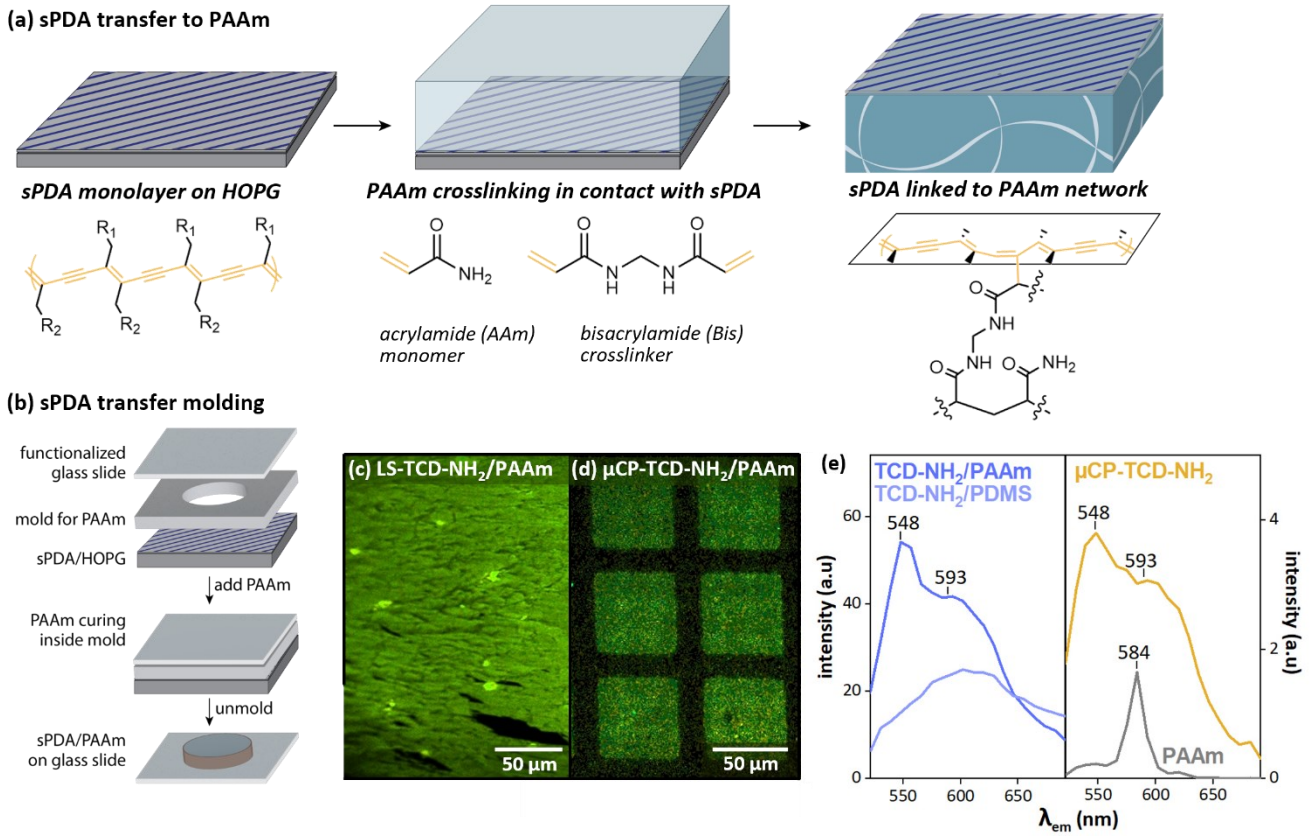

Figure 3. (a) Transfer of sPDA on HOPG to PAAm by in situ crosslinking. (b) Experimental setup for sPDA transfer. (c,d) Fluorescence images of (c) LS-TCD-NH_2/PAAm and (d) µCP-TCD-NH_2/PAAm. (e,f) Fluorescence spectra of sPDA-functionalized and bare PAAm.

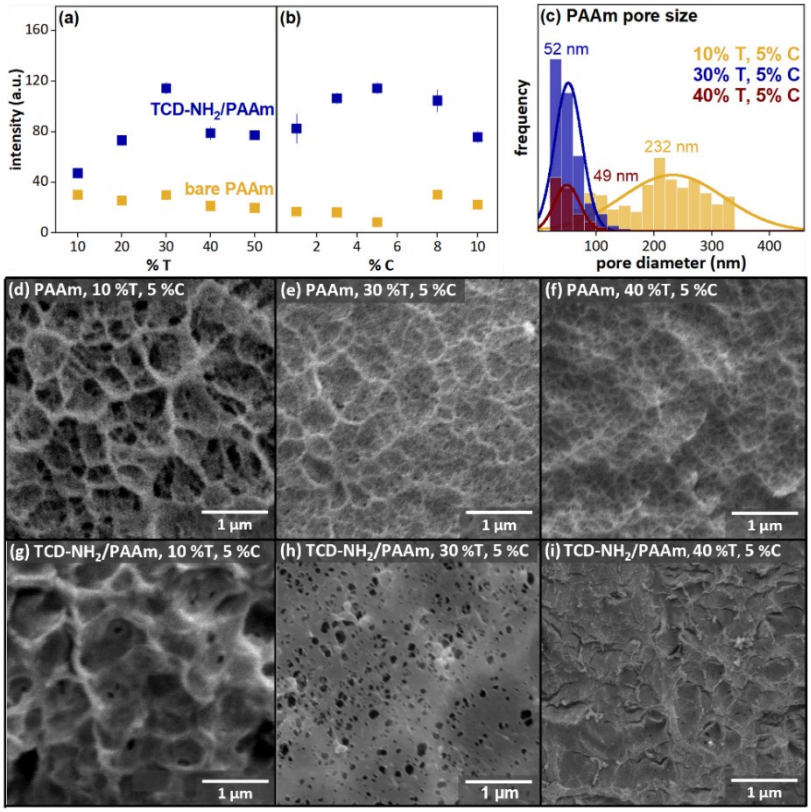

Figure 4. Fluorescence emission intensity of PAAm gels with varied (a) %T (mass % total acrylate in gel), and (b) %C (mass % crosslinker *vs.* total acrylate). (c) PAAm pore diameters calculated from cryoEM image analysis. (d–i) CryoEM images of (d–f) unfunctionalized PAAm and (g–i) TCD-NH_2/PAAm, illustrating differences in pore structure and texture with variation in %T and functionalization state.

polymerized network at the surface that includes not only the sPDA but PAAm oligomers that react with the sPDA, changing the near-surface pore structure. At larger scales, the relationship between the surface layer and the underlying gel structure is in some cases evident based on tearing and/or perforation of the surface layer (see Supporting Information, Figures S3 and S4).

Heterogeneities in the porous architecture (Figure 4) would have the potential to impact sPDA transfer by varying local reactant concentrations, and thus $p_{rxn,AAm}$ (Figure 5a). Previous literature has demonstrated that in these polymerization reactions, early stages of the reaction produce higher-density particles rich in Bis crosslinker, with diameters on the order of hundreds of nm.[35-36] In the final stages of the reaction, particles then become loosely crosslinked to other particles through fibers rich in AAm.[12-13] Increases in crosslinker or acrylate group concentration can produce more tightly crosslinked networks in the initial stage of polymerization, producing larger voids.[12,36-39]

In the context of sPDA transfer, PAAm network heterogeneities could result in local strong crosslinking to the sPDA monolayer in some regions, and more limited crosslinking in others. Visual inspection of fluorescence images of TCD-NH_2/PAAm illustrate speckling patterns that vary with %T (Figure 5b, see Supporting Information Figure S5 for larger images). Unfunctionalized PAAm produces much weaker fluorescence emission overall, however, speckling is visible for 40 and 50 %T gels (Figure 5c), at scales similar to those observed for functionalized surfaces. These observations may be consistent with the interpretation that one source of heterogeneities in sPDA transfer is heterogeneities in local PAAm gel structure (Figure 5d).

Relative intensities of longer- and shorter-wavelength PDA emission peaks also shift with increasing %T (Figure 5b, histograms), producing visible differences in color, plotted here using a cylindrical coordinate system that converts red, blue, and green components into linear coordinates from 0 to 360. Reasons for these shifts are not currently well-understood, but may relate to differences in torsion on the PDA backbone based on crosslinking density.

To quantify local differences in sPDA fluorescence intensity, we segmented images into high- and low-intensity pixel sets (segmentation examples for 20 and 30 %T in Figure 5e), and extracted fluorescence intensities separately for high- and low-intensity pixels (Figure 5f). We then used models of transfer developed previously[32] for PDMS (Figure 5a,g) to relate these differences in PDA emission to differences in transfer, and to estimate differences in sPDA crosslinking to the PAAm network (Figure 5h,i).

Our models for sPDA crosslinking and exfoliation onto a bulk polymer[32] do not depend directly on the chemistry of the bulk polymer. The model (Figure 5a, see Supporting Information for more extensive discussion) relates the per-PDA-unit probability of reaction with the bulk polymer (p_{rxn}) and

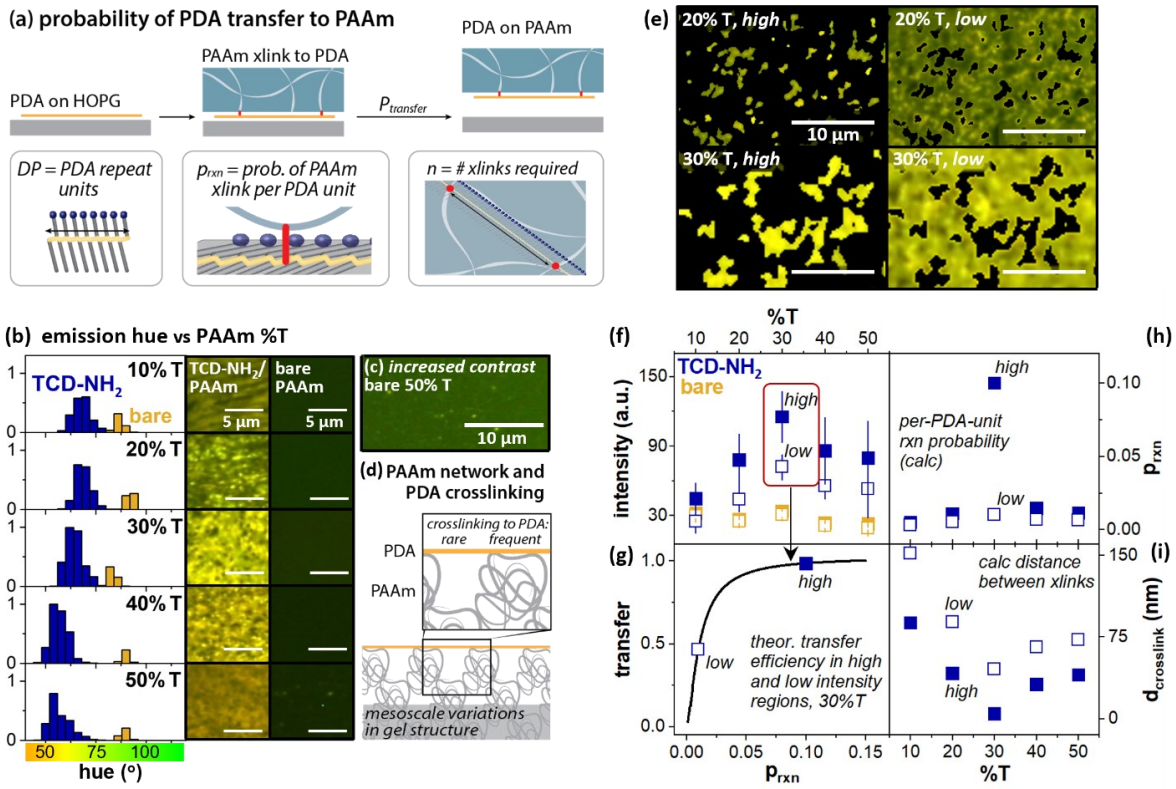

Figure 5. (a) Illustration of probability of transfer, in relationship to local PAAm network density. (b) Fluorescence images of TCD-NH_2/PAAm and bare PAAm, with histograms of pixels at each hue, illustrating shift with %T. (c) Image of bare PAAm prepared at 50 %T with increased contrast, showing faint speckling. (d) Illustration of relationship between heterogeneous PAAm network structure and variability in crosslinking to PDA. (e) Illustration of pixel intensity variations for 'high' and 'low'-intensity pixels at 20 %T and 30 %T. (f) Fluorescence emission for high and low intensity pixels in images of bare PAAm (gold) and TCD-NH_2/PAAm (blue) across the tested range of %T. (g,h) Projected differences in probability of reaction per PDA unit (P_{rxn}) and (i) average distance between crosslinks ($d_{crosslink}$), for the range of %T tested. Panel (a) adapted from ref 32 with permission. Copyright 2022 American Chemical Society.

number of crosslinks required for sPDA transfer (n) to the percentage of the sPDA monolayer projected to transfer ($P_{transfer}$), given the population of observed sPDA polymer lengths (DP) on HOPG. Here, we are using TCD-NH_2 sPDAs structurally equivalent to those used in the previous study[32] (same DP), and would expect the same number of crosslinks to be required to exfoliate the sPDAs (same n). Thus, if we observe a similar extent of transfer (calculated based on PDA fluorescence emission), the model would still predict the per-PDA reaction probability (p_{rxn}).

If we hypothesize that the brightest regions observed in TCD-NH_2/PAAm transfer experiments (Figure 4d, filled blue markers) correspond to complete monolayer transfer, high-intensity regions in 30 %T transfers represent this condition. Low-intensity regions (empty blue markers) in the same samples have emission intensities ~50% those of the high-intensity regions, after correcting for background emission from bare PAAm (yellow markers; blue markers indicate functionalized surface values after background subtraction), and would represent, on average, ~50% transfer. We mapped low and high-intensity pixels onto the transfer model developed previously (Figure 5e, see Supporting Information Figures S6 and S7 for details), which relates transfer efficiency with p_{rxn}. Figure 5f shows calculated p_{rxn} values for high and low-intensity regions across the tested range of %T; Figure 5g shows the theoretical transfer efficiency for 30%T/5%C formulation based on values in Figure 5f. This approach suggests that in regions with the highest transfer efficiency, p_{rxn} may be as high as 0.1, corresponding to an average distance between crosslinks of 10 monomers (5 nm), in highly crosslinked areas. However, in the low-intensity areas of similar samples, this method predicts ~50 nm between crosslinks, similar to average PAAm pore diameters calculated from cryoEM images in Figure 4c (Figure 5f,i). See Supporting Information for experimental details regarding analysis of fluorescence images for Figure 4a,b and 5f,i.

Using amine striped phases to control DNA adsorption. The linear patterns of amines on the hydrogel surface offer a means of controlling adsorption, and perhaps ultimately orientation, of complex biomolecules including DNA (Figure 6). Here, we tested two amine sPDAs, as well as amphiphiles with carboxylic acid and hydroxyl headgroups (Figure 6a). The model in Figure 6b illustrates the relative scale of a double-stranded DNA (dsDNA) helix and the sPDA surface pattern. Here, we examined the capacity of the surfaces to control DNA adsorption, using long dsDNA isolated from salmon sperm, with average helix lengths 2000 base pairs. DNA was first incubated with the intercalating fluorophore ethidium bromide (EtBr, see Experimental Methods for details), to produce fluorescent labeling along the contour length of each helix. EtBr–DNA complexes were then exposed to unfunctionalized and functionalized PAAm surfaces. Figure 6c shows μCP-TCD-NH_2/PAAm before (left) and after (right)

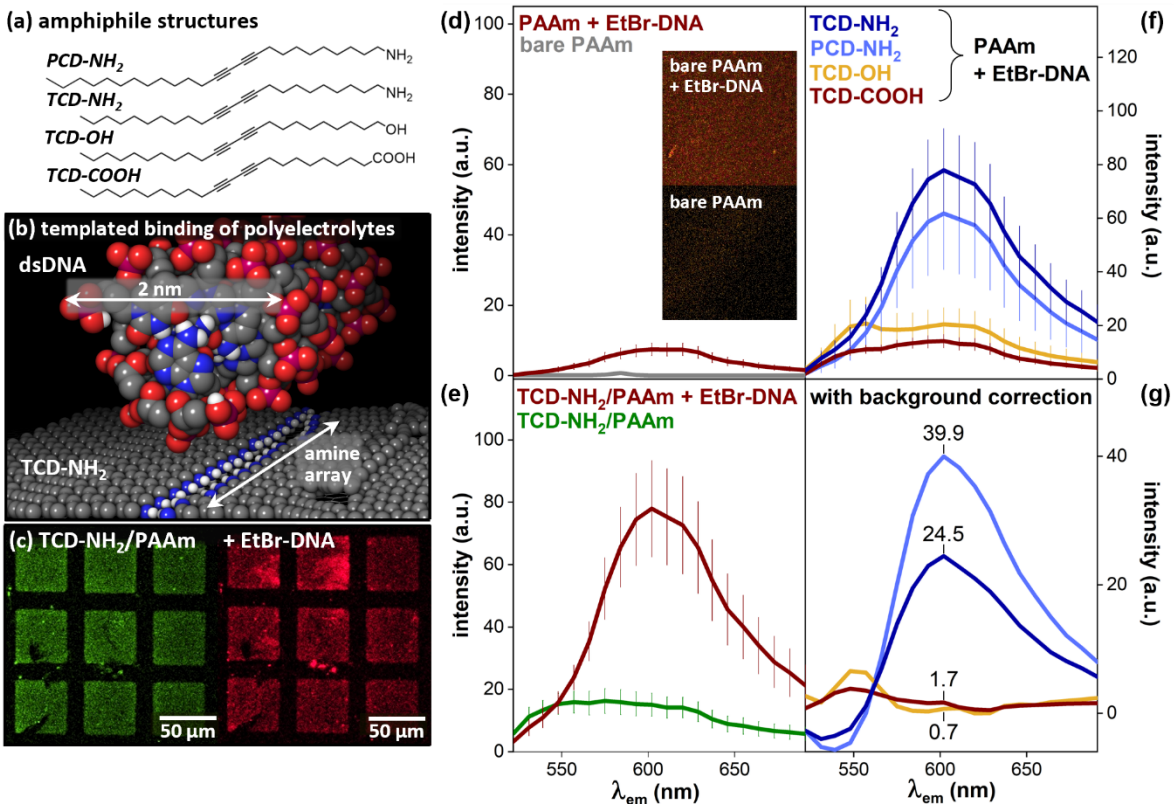

Figure 6. (a) Structures of polymerizable amphiphiles tested for DNA binding on sPDA/PAAm surfaces. (b) Molecular model illustrating relative scales of dsDNA and surface-patterned amines in sPDA. (c) Fluorescence images of TCD-NH_2/PAAm without (left) and with (right) exposure to EtBr-DNA. (d) Fluorescence spectra of bare PAAm with and without exposure to EtBr-DNA. (e) Fluorescence spectra of TCD-NH_2/PAAm without (green) and with (red) exposure to EtBr–DNA. (f) Composite fluorescence spectra from sPDA/PAAm substrates with amine (light and dark blue) carboxylic acid (red) or hydroxyl (gold) surface patterns, exposed to EtBr–DNA. (g) Spectra from (f) with background subtraction.

exposure to EtBr–DNA, illustrating the appearance of red fluorescence in the amine-patterned areas.

To quantify binding of DNA to the surface-patterned PAAm, we acquired fluorescence emission spectra from bare and functionalized PAAm with and without exposure to EtBr–DNA. Figure 6d illustrates that exposure of bare PAAm to EtBr–DNA, followed by a standard washing protocol (see Experimental Methods) produces modest fluorescence emission near 600 nm, in the spectral region associated with EtBr emission. Figure 6d (inset) illustrates swatches of bare PAAm without (top) and with (bottom) exposure to EtBr. Figure 6e shows emission from TCD-NH_2/PAAm without (green) and with (red) exposure to EtBr–DNA, with the same vertical scale used for the bare PAAm graph in Figure 6d.

We then examined EtBr–DNA binding to a set of sPDA-functionalized PAAm surfaces (monomer structures shown in Figure 6a), to test the impacts of specific functional groups displayed at the interface. Following exposure to EtBr–DNA at the same concentration (Figure 6f), amine-functionalized surfaces (TCD-NH_2 and PCD-NH_2) exhibit much greater DNA adsorption, than hydroxyl (TCD-OH) or carboxylic acid (TCD-COOH) functionalized surfaces. Figure 6g shows emission spectra with the sPDA, and PAAm+EtBrDNA background subtracted, illustrating the up to 40-fold increase in emission intensity at the EtBr maximum associated with amine-functionalized surfaces in contrast with OH or COOH-functionalized surfaces. See Supporting Information Figure S8 for more details regarding spectral subtraction. EtBr fluorescence intensity is strongly dependent on intercalation into dsDNA,[40] pointing to retention of the dsDNA structure when bound to the sPDA-functionalized PAAm. To further examine this point, we carried out experiments in which dsDNA (without EtBr) was adsorbed to PCD-NH_2/PAAm substrates, and subsequently exposed to EtBr (see Supporting Information Figure S9); EtBr was also capable of intercalation into DNA following adsorption to PCD-NH_2/PAAm, again pointing to the presence of dsDNA on the surface.

CONCLUSIONS

Here, we have demonstrated the capability to generate nanometer-resolution patterns of functional groups on HOPG, which can then be transferred to an amorphous acrylate hydrogel surface, and to use the patterned functional groups to direct surface adsorption of DNA. By extension, this approach may ultimately be useful in applications ranging from chromatography to hybrid nanomaterial design, taking advantage of this new class of ordered/amorphous interfaces.

EXPERIMENTAL METHODS

See Supporting Information for more detailed Materials and Experimental Methods.

Materials. See Supporting Information.

Langmuir-Schaefer transfer. Unless otherwise stated in the manuscript, monolayers of TCD-NH_2, PCD-NH_2, TCD-OH and TCD-COOH were prepared *via* a Langmuir-Schaefer conversion process we have reported previously,[16-17,22] using a custom-built temperature-controlled transfer stage.[22] The stage was utilized in conjunction with a MicroTrough XL Langmuir–Blodgett trough (Kibron Inc., Helsinki, Finland). HOPG substrates were mounted on standard 12-mm diameter stainless-steel AFM specimen discs and positioned on a magnet recessed in the temperature-controlled stage. Conductive carbon tape was used to affix the HOPG to the specimen disk surface to ensure temperature uniformity across the substrate surface. The temperature of the substrate was measured using a thermocouple prior to dipping. Films of each amphiphile were assembled at the air–water interface by depositing the appropriate amount of a 0.75 mg/mL amphiphile solution in chloroform, on a subphase comprised of 40 mM $CaCl_2$ in Milli-Q water, maintained at 30 °C. Barriers were then swept inward at 6.23 mm/min to achieve the target mean molecular area (MMA); the trough feedback mechanism was set to maintain the target MMA. HOPG substrates were freshly cleaved, mounted on the thermally controlled stage, set at either 25 °C, for transfer of monolayers containing circular vacancies, or 70 °C for full coverage monolayers, then lowered (at 2 mm/min) into contact with the subphase. Contact was maintained for 2 min, and the HOPG was then lifted out of contact at a rate of 2 mm/min. After contact with the subphase was broken, HOPG substrates were blown dry with UHP N_2. Finally, unless otherwise stated in the manuscript, HOPG substrates were placed under a hand-held UV lamp (254 nm, 8 W) for 1 h with ~10 cm between the lamp and the substrate to induce diyne photopolymerization.

Cryo-EM imaging. *Sample preparation.* Prior to imaging, samples were placed in 10% *v/v* ethanol/Milli-Q water for 10 min; ethanol is used as a cryoprotectant[41] to minimize crystalline ice formation during cryo-fixation. Samples were then prepared by cutting irregular edges off, producing flat surfaces with final dimensions of *ca.* 0.5 cm × 0.5 cm. Each sample was then mounted on a flat specimen holder with optimal cutting temperature (OCT) cryo embedding media. Mounted samples in the specimen holder were clamped to an ALT118 brass Gatan plunger (Gatan, Oxford, UK) and immersed in a liquid nitrogen slush under ambient pressure until equilibrated. Samples were then cryo-transferred into the Gatan Alto 2500 preparation chamber, preset to -180 °C. Cross-sectional samples were prepared using a vise clamp holder and a surgical scalpel to fracture the sample at the base. Subsequently, the sample was transferred onto the Nova SEM cryo stage, which was pre-cooled to -85 °C for sublimation of ice. Sublimation was monitored until the sample surface was frost free. When sublimation was complete, samples were returned to the cryo preparation chamber for sputter-coating with a Pt target for 45–60 s; a 45 s sputtering time was used, unless otherwise specified in the manuscript. *Sample imaging.* Following cryo-fixation and sputtering, samples were imaged using a FEI Nova Nano SEM (FEI, Thermo Fisher Scientific, Hillsboro, OR). The SEM chamber temperature was maintained at -140 °C, and imaging was performed using a 5 kV beam with a spot size of 5. Electrons were collected using an Everhart Thornley Detector for low magnification images, and an immersion-mode through-the-lens detector for high magnification images.

Covalent transfer of PDA striped phases from HOPG to PAAm. Surfaces were grafted with TMS-PMA, using previously reported procedures,[42] see detailed Experimental Methods in Supporting Information for additional description. Polyacrylamide (PAAm) hydrogels were prepared using previously reported formulations,[43] described in more detail in the Supporting Information. For PAAm curing and sPDA monolayer exfoliation, the sPDA/HOPG samples were first covered with rubber molds 2 cm in diameter and 2 mm thick (Ted Pella, Inc.) with an 0.5 cm × 0.5 cm square cut to fit the HOPG area. Double sided clear tape (3M Scotch) was used to

create a temporary seal between the HOPG and the rubber mold, preventing hydrogel precursor solution from leaking. Precursor solution was degassed by bubbling with UHP N_2 for 5 min prior to gelation. A 10% *w/v* solution of the ammonium persulfate (APS) initiator was prepared in Milli-Q water. The catalyst, tetramethylenediamine (TEMED), was used as received. To initiate gelation, 10 μL of the APS solution, 1 μL of TEMED, and 989 μL of the chosen AAm/Bis precursor solution were mixed by gentle pipetting, and vortexed thoroughly for 30 s. Subsequently, 100 μL of the precursor mixture was cast on the prepared HOPG substrates and immediately capped with a 1 cm^2 vinyl-functionalized glass coverslip, ensuring that the entire HOPG surface was covered by the acrylamide mixture. Hydrogels were cured at room temperature for 15 min, and stored in Milli-Q water, unless otherwise specified.

DNA adsorption experiments. Initially, a 1 mg/mL stock solution (2500 μM) of ethidium bromide (EtBr) in Milli-Q water was prepared and diluted to 100 μM with Milli-Q water. The ratio of double stranded DNA (dsDNA) sodium salt from salmon testes (average 2000 base pairs, equivalent to 680 nm double strand helix contour length) to EtBr was adjusted to produce a molar ratio of one dsDNA strand per 80 EtBr molecules (DNA-EtBr). For example, to prepare a 1 μM DNA and 80 μM EtBr solution, 1.36 mg of dsDNA were weighed into a vial along with 800 μL of a 100 μM EtBr solution and 200 μL of Milli-Q water to make a final volume of 1 mL. The solution was mixed thoroughly by vortex for at least 10 min and allowed to equilibrate overnight. DNA solutions were stored at 4 °C when not in use. To quantify DNA–EtBr adsorption on sPDA/PAAm substrates, 30 μL of DNA–EtBr solution were cast on functionalized or unfunctionalized PAAm substrates and incubated for 10 min in a petri dish protected from light and dust. Following incubation, the EtBr–DNA solution was carefully wicked off the PAAm surface using a Kimwipe. Samples were rinsed using a previously reported procedure[44] comprised of: two 20-s cycles of vortexing with 0.1% *w/v* SDS in Milli-Q water, followed by two 20-s cycles of vortexing with pure Milli-Q water. Samples were subsequently stored in Milli-Q water and analyzed within 1 h after exposure.

ASSOCIATED CONTENT

Supporting Information

Detailed experimental methods; larger AFM and SEM images illustrating LS assembly of striped phase films of TCD-NH_2 on HOPG; larger fluorescence microscopy images illustrating sPDA monolayers transferred to PAAm; larger cryoEM images of TCD-NH_2/PAAm, illustrating surface layer structure; larger fluorescence images of TCD-NH_2/PAAm with %T values ranging from 10–50%; Calculation of transfer probabilities of sPDA polymers; illustration of steps in background correction for DNA adsorption experiments. This material is available free of charge via the Internet at http://pubs.acs.org.

Notes

The authors declare no competing financial interests.

AUTHOR INFORMATION

Corresponding Author
Shelley A. Claridge – *Department of Chemistry and Weldon School of Biomedical Engineering, Purdue University, West Lafayette, Indiana 47907, United States; orcid.org/0000- 0002-8599-0589; Phone: 765-494-6070; Email: claridge@ purdue.edu*
Juan C. Arango – *Department of Chemistry, Purdue University, West Lafayette, Indiana 47907, United States*
Laura O. Williams – *Department of Chemistry, Purdue University, West Lafayette, Indiana 47907, United States*
Anni Shi – *Department of Chemistry, Purdue University, West Lafayette, Indiana 47907, United States*
Anamika Singh – *Department of Chemistry, Purdue University, West Lafayette, Indiana 47907, United States*
Emmanuel K. Nava – *Department of Chemistry, Purdue University, West Lafayette, Indiana 47907, United States*
Racheal V. Fisher – *Department of Chemistry, Purdue University, West Lafayette, Indiana 47907, United States*
Joseph A. Garfield – *Department of Chemistry, Purdue University, West Lafayette, Indiana 47907, United States*

ACKNOWLEDGMENT

SAC acknowledges support through an NSF grant, NSF-CHE-MSN 2108966. Instrumentation in the Purdue Imaging Facility was utilized for optical microscopy experiments, and instruments in the Purdue Electron Microscopy Facility were used for SEM imaging.

REFERENCES

1. Slaughter, B. V.; Khurshid, S. S.; Fisher, O. Z.; Khademhosseini, A.; Peppas, N. A. Hydrogels in Regenerative Medicine. *Adv. Mater.* **2009,** *21*, 3307-3329.
2. Caliari, S. R.; Burdick, J. A. A Practical Guide to Hydrogels for Cell Culture. *Nat. Methods* **2016,** *13*, 405-414.
3. Madl, C. M.; Heilshorn, S. C. Engineering Hydrogel Microenvironments to Recapitulate the Stem Cell Niche. *Annu. Rev. Biomed. Eng.* **2018,** *20*, 21-47.
4. Nichols, A. V.; Krauss, R. M.; Musliner, T. A. Nondenaturing Polyacrylamide Gradient Gel Electrophoresis. *Methods Enzymol.* **1985,** *128*, 417-431.
5. Bjellqvist, B.; Pasquali, C.; Ravier, F.; Sanchez, J.-C.; Hochstrasser, D. A Nonlinear Wide-Range Immobilized pH Gradient for Two-Dimensional Electrophoresis and Its Definition in a Relevant pH Scale. *Electrophoresis* **1993,** *14*, 1357-1365.
6. Yang, C.; DelRio, F. W.; Ma, H.; Killaars, A. R.; Basta, L. P.; Kyburz, K. A.; Anseth, K. S. Spatially Patterned Matrix Elasticity Directs Stem Cell Fate. *Proc. Natl. Acad. Sci. U. S. A.* **2016,** *113*, 4439-4445.
7. Raymond, S.; Weintraub, L. Acrylamide Gel as a Supporting Medium for Zone Electrophoresis. *Science* **1959,** *130*, 711.
8. Davis, B. J. Disc Electrophoresis - II. Method and Application to Human Serum Proteins. *Ann. N. Y. Acad. Sci.* **1964,** *121*, 404-427.
9. Ornstein, L. Disc Electrophoresis - I. Background and Theory. *Ann. N. Y. Acad. Sci.* **1964,** *121*, 321-349.
10. Pandey, A.; Mann, M. Proteomics to Study Genes and Genomes. *Nature* **2000,** *405*, 837-846.
11. Engler, A. J.; Sen, S.; Sweeney, H. L.; Discher, D. E. Matrix Elasticity Directs Stem Cell Lineage Specification. *Cell* **2006,** *126*, 677-689.
12. Weiss, N.; Van Vliet, T.; Silberberg, A. Influence of Polymerization Initiation Rate on Permeability of Aqueous Polyacrylamide Gels. *J. Polym. Sci., Polym. Phys. Ed.* **1981,** *19*, 1505-1512.
13. Weiss, N.; Silberberg, A. Inhomogeneity of Polyacrylamide Gel Structure from Permeability and Viscoelasticity. *Br. Polym. J.* **1977,** *9*, 144-150.
14. Davis, T. C.; Bechtold, J. O.; Shi, A.; Lang, E. N.; Singh, A.; Claridge, S. A. One Nanometer Wide Functional Patterns

with a Sub-10 Nanometer Pitch Transferred to an Amorphous Elastomeric Material. *ACS Nano* **2021,** *15*, 1426-1435.
15. Bang, J. J.; Rupp, K. K.; Russell, S. R.; Choong, S. W.; Claridge, S. A. Sitting Phases of Polymerizable Amphiphiles for Controlled Functionalization of Layered Materials. *J. Am. Chem. Soc.* **2016,** *138*, 4448-4457.
16. Davis, T. C.; Bang, J. J.; Brooks, J. T.; McMillan, D. G.; Claridge, S. A. Hierarchical Noncovalent Functionalization of 2D Materials by Controlled Langmuir-Schaefer Conversion. *Langmuir* **2018,** *34*, 1353-1362.
17. Bang, J. J.; Porter, A. G.; Davis, T. C.; Hayes, T. R.; Claridge, S. A. Spatially Controlled Noncovalent Functionalization of 2D Materials Based on Molecular Architecture. *Langmuir* **2018,** *34*, 5454-5463.
18. Villarreal, T. A.; Russell, S. R.; Bang, J. J.; Patterson, J. K.; Claridge, S. A. Modulating Wettability of Layered Materials by Controlling Ligand Polar Headgroup Dynamics. *J. Am. Chem. Soc.* **2017,** *139*, 11973-11979.
19. Shi, A.; Villarreal, T. A.; Singh, A.; Hayes, T. R.; Davis, T. C.; Brooks, J. T.; Claridge, S. A. Plenty of Room at the Top: A Multi-Scale Understanding of nm-Resolution Polymer Patterning on 2D Materials. *Angew. Chem., Int. Ed.* **2021,** *60*, 25436-25444.
20. Davis, T. C.; Bechtold, J. O.; Hayes, T. R.; Villarreal, T. A.; Claridge, S. A. Hierarchically Patterned Striped Phases of Phospholipids: Toward Controlled Presentation of Carbohydrates. *Faraday Discuss.* **2019,** *219*, 229-243.
21. Bang, J. J.; Porter, A. G.; Davis, T. C.; Hayes, T. R.; Claridge, S. A. Spatially Controlled Noncovalent Functionalization of 2D Materials Based on Molecular Architecture *Langmuir* **2018,** *34*, 5454-5463.
22. Hayes, T. R.; Bang, J. J.; Davis, T. C.; Peterson, C. F.; McMillan, D. G.; Claridge, S. A. Multimicrometer Noncovalent Monolayer Domains on Layered Materials through Thermally Controlled Langmuir-Schaefer Conversion for Noncovalent 2D Functionalization. *ACS Appl. Mater. Interf.* **2017,** *9*, 36409–36416.
23. Russell, S. R.; Davis, T. C.; Bang, J. J.; Claridge, S. A. Spectroscopic Metrics for Alkyl Chain Ordering in Lying-Down Noncovalent Monolayers of Diynoic Acids on Graphene. *Chem. Mater.* **2018,** *30*, 2506-2514.
24. Hayes, T. R.; Lang, E. N.; Shi, A.; Claridge, S. A. Large-Scale Noncovalent Functionalization of 2D Materials through Thermally Controlled Rotary Langmuir-Schaefer Conversion. *Langmuir* **2020,** *36*, 10577-10586.
25. Hayes, T. R.; Bang, J. J.; Davis, T. C.; Peterson, C. F.; McMillan, D. G.; Claridge, S. A. Multimicrometer Noncovalent Monolayer Domains on Layered Materials through Thermally Controlled Langmuir-Schaefer Conversion for Noncovalent 2D Functionalization. *ACS Appl. Mater. Interf.* **2017,** *9*, 36409-36416.
26. Goronzy, D. P.; Ebrahimi, M.; Rosei, F.; Arramel; Fang, Y.; De Feyter, S.; Tait, S. L.; Wang, C.; Beton, P. H.; Wee, A. T. S.; Weiss, P. S.; Perepichka, D. F. Supramolecular Assemblies on Surfaces: Nanopatterning, Functionality, and Reactivity. *ACS Nano* **2018,** *12*, 7445-7481.
27. Choong, S. W.; Russell, S. R.; Bang, J. J.; Patterson, J. K.; Claridge, S. A. Sitting Phase Monolayers of Polymerizable Phospholipids Create Dimensional, Molecular-Scale Wetting Control for Scalable Solution Based Patterning of Layered Materials. *ACS Appl. Mater. Interf.* **2017,** *9*, 19326-19334.
28. Porter, A. G.; Ouyang, T.; Hayes, T. R.; Biechele-Speziale, J.; Russell, S. R.; Claridge, S. A. 1-nm-Wide Hydrated Dipole Arrays Regulate AuNW Assembly on Striped Monolayers in Nonpolar Solvent. *Chem* **2019,** *5*, 2264-2275.
29. Russell, S. R.; Davis, T. C.; Clark, M. G.; Hayes, T. R.; Claridge, S. A. Displaceable Templates with Sub-10 nm Periodicity Activate and Direct Epitaxial Assembly of Complex Aromatic Molecules. *Chem. Mater.* **2020,** *32*, 2552-2560.
30. Bechtold, J. O.; Arango, J. C.; Shi, A.; Singh, A.; Claridge, S. A. Striped Poly(Diacetylene) Monolayers Control Adsorption of Polyelectrolytes and Proteins on 2D Materials and Elastomers. *ACS Appl. Nano Mater.* **2021,** *4*, 7037-7046.
31. Lang, E. N.; Porter, A. G.; Ouyang, T.; Shi, A.; Hayes, T. R.; Davis, T. C.; Claridge, S. A. Oleylamine Impurities Regulate Temperature-Dependent Hierarchical Assembly of Ultranarrow Gold Nanowires on Biotemplated Interfaces. *ACS Nano* **2021,** *15*, 10275-10285.
32. Shi, A.; Singh, A.; Williams, L. O.; Arango, J. C.; Claridge, S. A. Nanometer-Scale Precision Polymer Patterning of PDMS: Multiscale Insights into Patterning Efficiency Using Alkyldiynamines. *ACS Appl. Mater. Interf.* **2022,** *14*, 22634-22642.
33. Green, M. R.; Sambrook, J., Polyacrylamide Gel Electrophoresis. In *Cold Spring Harbor Protocols*, Cold Spring Harbor Laboratory Press: 2020; pp 525-532.
34. Ruchel, R.; Steere, R. L.; Erbe, E. F. Transmission-Electron Microscopic Observations of Freeze-Etched Polyacrylamide Gels. *J. Chromatogr.* **1978,** *166*, 563-575.
35. Righetti, P. G.; Caglio, S. On the Kinetics of Monomer Incorporation into Polyacrylamide Gels, as Investigated by Capillary Zone Electrophoresis. *Electrophoresis* **1993,** *14*, 573-582.
36. Stellwagen, N. C. Electrophoresis of DNA in Agarose Gels, Polyacrylamide Gels and in Free Solution. *Electrophoresis* **2009,** *30*, S199-S195.
37. Stellwagen, N. C. Apparent Pore Size of Polyacrylamide Gels: Comparison of Gels Cast and Run in Tris-Acetate-EDTA and Tris-Borate-EDTA Buffers. *Electrophoresis* **1998,** *19*, 1542-1547.
38. Margolis, J.; Wrigley, C. W. Improvement of Pore Gradient Electrophoresis by Increasing the Degree of Crosslinking at High Acrylamide Concentrations. *J. Chromatogr.* **1975,** *106*, 204-209.
39. Campbell, W. P.; Wrigley, C. W.; Margolis, J. Electrophoresis of Small Proteins in Highly Concentrated and Crosslinked Polyacrylamide Gradient Gels. *Anal. Biochem.* **1983,** *129*, 31-36.
40. Olmsted, J.; Kearns, D. R. Mechanism of Ethidium Bromide Fluorescence Enhancement on Binding to Nucleic Acids. *Biochem.* **1977,** *16*, 3647-3654.
41. Aston, R.; Sewell, K.; Klein, T.; Lawrie, G.; Grøndahl, L. Evaluation of the Impact of Freezing Preparation Techniques on the Characterisation of Alginate Hydrogels by Cryo-SEM. *Eur. Polym. J.* **2016,** *82*, 1-15.
42. Yuk, H.; Zhang, T.; Lin, S.; Parada, G. A.; Zhao, X. Tough Bonding of Hydrogels to Diverse Non-Porous surfaces. *Nat. Mater.* **2016,** *15*, 190-196.
43. Tse, J. R.; Engler, A. J. Preparation of Hydrogel Substrates with Tunable Mechanical Properties. *Current Protocols in Cell Biology* **2010,** *47*, 10.16.11-10.16.11.
44. Das, J.; Huh, C.-H.; Kwon, K.; Park, S.; Jon, S.; Kim, K.; Yang, H. Comparison of the Nonspecific Binding of DNA-Conjugated Gold Nanoparticles between Polymeric and Monomeric Self-Assembled Monolayers. *Langmuir* **2009,** *25*, 235-241.

TOC graphic goes here